

Metal coordination study at Ag and Cd sites in crown thioether complexes through DFT calculations and hyperfine parameters

Rafael R. do Nascimento¹ · Filipe C. D. A. Lima¹ · Marcos B. Gonçalves^{1,2} · Leonardo A. Errico^{3,4} · Mario Rentería³ · Helena M. Petrilli¹

Received: 4 January 2015 / Accepted: 9 March 2015
© Springer-Verlag Berlin Heidelberg 2015

Abstract Structural and electronic properties of [C₁₂H₂₄S₆X], [C₁₃H₂₆S₆OX], and [C₁₄H₂₈S₆OX] (X: Ag⁺, Cd²⁺) crown thioether complexes were investigated within the framework of the density functional theory (DFT) using the projector augmented wave (PAW) method. The theoretical results were compared with time-differential perturbed γ - γ angular correlations (TDPAC) experiments reported in the literature using the ¹¹¹Ag→¹¹¹Cd probe. In the case of X=Ag⁺, a refinement of the structure was performed and the predicted equilibrium structures compared with available X-ray diffraction experimental data. Structural distortions induced by replacing Ag⁺ with Cd²⁺ were investigated as well as the electric-field gradient (EFG) tensor at the Cd²⁺ sites. Our results suggest that the EFG at Cd²⁺ sites corresponds to the Ag⁺ coordination sphere structure, i.e., before the structural relaxations of the molecule with X=Cd²⁺ are completed. The results are discussed in terms of the characteristics of the TDPAC ¹¹¹Ag→¹¹¹Cd probe and the time window of the measurement, and provide an interesting tool with which to probe molecular relaxations.

Keywords Crown thioether metal complexes · Hyperfine interactions · Electric field gradient · Perturbed angular correlations · Density functional calculations · Silver · Cadmium

Introduction

Thiacrown ligands are important compounds with applications in nanotechnology, environmental chemistry, pharmacology and toxicology due to their ability to chelate metallic ions [1–3]. The choice of these macrocyclic ligands is based on the inherent selectivity of thioether groups to soft and soft-mild transition metals, such as Ag⁺, Cd²⁺, Pb²⁺, Cu²⁺, and Zn²⁺ [4]. Several studies aiming to develop applications for thiacycrown ligands have been reported, including Hg²⁺ chemosensor in water [5], competitive liquid–liquid solvent metal chelation [4], stabilizing unstable oxidation states such as Pd³⁺, Au²⁺ and Ag²⁺ [6, 7], antitumor compounds [8–12] and protein kinase inhibitors [13]. Since the hazardous effects of free metal ions in the human body are numerous [14] (e.g., amyotrophic lateral sclerosis, kidney malfunction, cancer, Alzheimer's and Parkinson's diseases), a natural application of thiacycrown ligands is in this area. However, structural and stability characterization of thiacycrown metal complexes in biological environments is not straightforward. However, in special cases, the electric-field-gradient (EFG) tensor at a certain probe site provides a local and very accurate fingerprint of metal coordination. The EFG can be measured through different hyperfine techniques such as nuclear quadrupole resonance (NQR), nuclear magnetic resonance (NMR), Mössbauer spectroscopy (MS), and time-differential perturbed angular γ - γ correlation (TDPAC) [15]. Experimental determinations of the EFG have been used successfully to address a wide range of studies with biological applications

✉ Helena M. Petrilli
hmpetril@if.usp.br

¹ Instituto de Física, Universidade de São Paulo, Rua do Matão Travessa R, Nr.187, Cidade Universitária, CP 66318, 05508-090 São Paulo, Brazil

² Departamento de Física, Universidade Tecnológica Federal do Paraná, 80230-901 Curitiba, Paraná, Brazil

³ Departamento de Física, Instituto de Física La Plata (IFLP, CCT-La Plata, CONICET-UNLP), Facultad de Ciencias Exactas, Universidad Nacional de La Plata, Casilla de Correo 67, 1900 La Plata, Argentina

⁴ Universidad Nacional del Noroeste de la Provincia de Buenos Aires (UNNOBA), Monteagudo 2772, PergaminoCP 2700Buenos Aires, Argentina

when combined with molecular modeling in the framework of the density functional theory (DFT) [16]. Recent characterization examples are: the coordination environment of the human copper chaperone HAH1 [17], the physical properties and coordination of metal sites in peptides [18], bisphosphonate derivatives as drugs for cancer inhibition [19], hydrogen bond patterns in potential antileukemic agents [20], and DNA mutations in mice infected with *Trypanosoma cruzi* [21].

A family of Ag-crown thioether complexes were studied through TDPAC using the ($^{111}\text{Ag} \rightarrow$) ^{111}Cd probe, aimed at potential applications as radiopharmaceuticals [22]. In 2005, Heinrich et al. [23] used a DFT approach in order to establish a simple model to correlate the EFGs with the specific metal coordination environments in these complexes. The calculations were performed at the Ag sites, although the TDPAC measurements were performed at the ^{111}Cd nucleus after the $^{111}\text{Ag} \rightarrow$ ^{111}Cd nuclear decay [24–26]. Since the EFG is very sensitive to anisotropic charge distribution close to the probe nucleus, this decay can induce electronic and structural changes in the host molecules that was not taken into account by Heinrich et al. [23].

In the present work, we report an ab initio DFT study of three crown thioether molecules, namely $[\text{C}_{12}\text{H}_{24}\text{S}_6\text{X}]^n$, $[\text{C}_{13}\text{H}_{26}\text{S}_6\text{OX}]^n$ and $[\text{C}_{14}\text{H}_{28}\text{S}_6\text{OX}]^n$, where X is Ag or Cd. In order to elucidate the chemical differences between Cd and Ag, theoretical EFG calculations in both metal sites (taking the structural and electronic changes induced by the Cd ion properly into account) were performed here and compared with the $^{111}\text{Ag} \rightarrow$ ^{111}Cd TDPAC experiments. Counterion influence, the role played by the environment, the electronic structure, and hyperfine properties of the metal complexes are discussed. By comparing theory and experiment we obtained a scenario for the local structure around the probe and discuss the molecular relaxation times.

Computational methods

The complexes selected for these studies are $[\text{C}_{12}\text{H}_{24}\text{S}_6\text{Ag}][\text{PF}_6]$, $[\text{C}_{13}\text{H}_{26}\text{S}_6\text{OAg}][\text{CF}_3\text{SO}_3]$ and $[\text{C}_{14}\text{H}_{28}\text{S}_6\text{OAg}][\text{BF}_4]$; the corresponding X-ray structures can be found in the literature [22, 27]. Figure 1 shows the 2D chemical structures without the counterion, namely $[\text{C}_{12}\text{H}_{24}\text{S}_6\text{X}]^n$, $[\text{C}_{13}\text{H}_{26}\text{S}_6\text{OX}]^n$ and $[\text{C}_{14}\text{H}_{28}\text{S}_6\text{OX}]^n$, where X stands for the metal ion (Ag^+ or Cd^{2+}) and n is the total charge of the complexes.

The EFG is a traceless symmetric tensor with components denoted by V_{ij} , defined by the second derivative of the Coulomb potential $V(r)$ at the nuclear site, as described in [28]. In the principal axis system, the traceless property assures that $V_{xx} + V_{yy} + V_{zz} = 0$, V_{xx} , V_{yy} and V_{zz} being the diagonal elements. The conventional choice is $|V_{xx}| \leq |V_{yy}| < |V_{zz}|$, hence V_{zz} is the largest eigenvalue of the tensor. Instead of

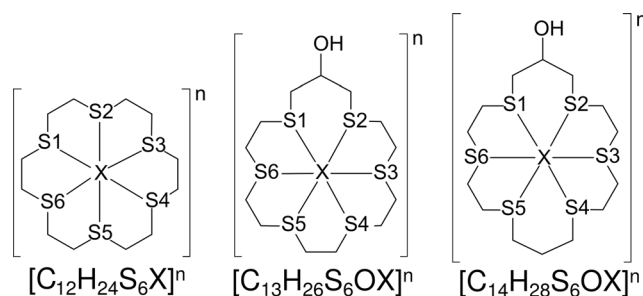


Fig. 1 The three crown thioether complexes $[\text{C}_{12}\text{H}_{24}\text{S}_6\text{X}]^n$, $[\text{C}_{13}\text{H}_{26}\text{S}_6\text{OX}]^n$ and $[\text{C}_{14}\text{H}_{28}\text{S}_6\text{OX}]^n$. X represents the metal site and n the total charge

specifying three diagonal elements, usually V_{zz} and the asymmetry parameter $\eta = (V_{xx} - V_{yy})/V_{zz}$ are reported. In the case of a pure-electric-quadrupole interaction (as in the case of the experiments that will be discussed here) the measured magnitudes are η and the nuclear quadrupole frequency ω_Q related to V_{zz} through $\omega_Q = eQV_{zz}/[4I(2I - 1)\hbar]$ [16]. Here, Q stands for the nuclear quadrupole moment of the sensitive TDPAC probe state, which is characterized by a nuclear spin quantum number I ($I = 5/2+$ for the 245 KeV excited state of ^{111}Cd , $Q = 0.83(13)$ b [29, 30], see Fig. 2) and e is the proton's charge. The EFG can be obtained from the charge density of the system using DFT calculations.

In order to solve the Kohn-Sham (KS) equations in the framework of the DFT [31, 32], the projector augmented wave (PAW) method as embodied in the Car-Parrinello (CP)-PAW code developed by Blöchl et al. [33, 34] was used. The PAW, an all-electron method, is able to accurately predict hyperfine properties [28, 33–36]. Instead of solving KS equations through matrix diagonalization, the CP scheme [37], with dampened motion, was used to determine the electronic structure and the atomic positions. The basis set is constituted by plane waves and localized wave functions, which preserves the information of the characteristic wave function nodal structure in the regions near the nuclei. PAW uses an “augmentation” approach, from the all-electron augmented

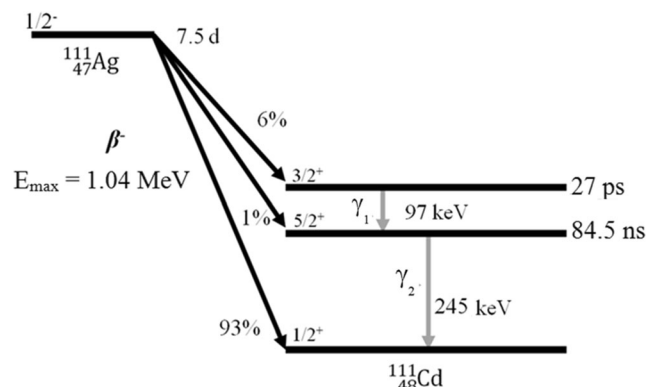


Fig. 2 Simplified nuclear decay scheme of ^{111}Ag [15]. The value of the nuclear quadrupole moment (Q) of the 245 keV excited state (0.83 b) was taken from the literature [29, 30]. The half-life of the $3/2+$ 342 keV and $5/2+$ 245 keV of ^{111}Cd are 27 ps and 84.5 ns, respectively [29, 30]

wave method, specified by the so-called projector functions. The PAW calculations were performed using one *s* projector function for hydrogen, and two *s*, two *p* and one *d* projector function for other atoms. The value of the plane waves and charge density cutoff energies are 30 Ry and 120 Ry, respectively. Exchange and correlation (E_{xc}) effects were treated using the Perdew, Burke and Ernzerhof (GGA-PBE) functional [38]. The choice of the projectors, the cutoff energy criteria, and E_{xc} functional were based on previous calculations [21, 24, 28, 39, 40], which also investigated EFG properties in molecules. All calculations were performed in the reciprocal space and the generated unit cell was chosen in order to be large enough to assure that the wave functions images did not interact with each other and decouple the spurious electrostatic interaction between molecules using a compensating charge background. As a consequence, the calculated molecules were isolated from the neighboring molecules simulating a gas phase environment. For the present calculations, unit cells with dimensions $14 \times 20 \times 20 \text{ \AA}^3$ for $[\text{C}_{12}\text{H}_{24}\text{S}_6\text{X}]$ and $17 \times 20 \times 20 \text{ \AA}^3$ for $[\text{C}_{13}\text{H}_{26}\text{S}_6\text{OX}]$ and $[\text{C}_{14}\text{H}_{28}\text{S}_6\text{OX}]$ were used. In these cases, the molecules are kept sufficiently far from each other (at least 6 \AA) [34].

The computational steps of the present study are summarized in Fig. 3, using $[\text{C}_{12}\text{H}_{24}\text{S}_6\text{X}]^n$ as an example. STEP I shows the experimentally determined structure of $[\text{C}_{12}\text{H}_{24}\text{S}_6\text{Ag}]^+$ (position 1) and STEP II shows the equilibrium structure predicted by CP-PAW optimization (Position 2). STEP III represents the moment when the $^{111}\text{Ag} \rightarrow ^{111}\text{Cd}$ nuclear decay takes place, i.e., replacement of the Ag^+ ion by the Cd^{2+} ion, on the Ag^+ coordination sphere (position 2) and prior to the structural changes induced by Cd. Finally, position 3 in STEP IV is obtained after structural optimization of position 2. This computational procedure was repeated for the other complexes studied here.

Results and discussion

Initially, computational studies on the Ag complexes were performed in order to investigate the influence of the

counterion on the structural distortions at the metal sites. The $[\text{C}_{12}\text{H}_{24}\text{S}_6\text{Ag}][\text{PF}_6]$ crystal [27] has three metal complexes and three $[\text{PF}_6]^-$ counterions per unit cell. Analogously, $[\text{C}_{13}\text{H}_{26}\text{S}_6\text{OAg}][\text{CF}_3\text{SO}_3]$ and $[\text{C}_{14}\text{H}_{28}\text{S}_6\text{OAg}][\text{BF}_4]$ crystals have two metal complexes and two counterions per unit cell [22]. In Ag-crown thioether complexes, the metal is coordinated by four S sites (equatorial distances), and two S longest distances (axial distances). From each crystal, a metal complex and the closest counterion were extracted to perform a full optimization of a neutral molecular system. The theoretical and experimental distances are shown in Table 1 (see Positions 1 and 2-CI), where qualitative good agreement between X-ray and optimized structures can be seen. The predicted S–Ag bond lengths were larger than the experimental bond lengths—a well-known characteristic of the GGA exchange correlation functional [38]. The only exception to this behavior was the S4–Ag bond length in $[\text{C}_{13}\text{H}_{26}\text{S}_6\text{OAg}][\text{CF}_3\text{SO}_3]$, which is reduced by about 6 %. On the other hand, the theoretically predicted bond lengths between the Ag and the counterion are reduced systematically with respect to the experimental bond lengths. In addition, the same complexes were investigated without the counterions, namely $[\text{C}_{12}\text{H}_{24}\text{S}_6\text{Ag}]^+$, $[\text{C}_{13}\text{H}_{26}\text{S}_6\text{OAg}]^+$ and $[\text{C}_{14}\text{H}_{28}\text{S}_6\text{OAg}]^+$, in order to determine the influence of the counterion on metal coordination. After the structural optimizations, all S–Ag bond lengths also increased up to 6 % with respect to the experimental data (see positions 1 and 2 in Table 1). In both cases, the correct metal coordination was found [22, 27], i.e., tetrahedral distorted for $[\text{C}_{13}\text{H}_{26}\text{S}_6\text{OAg}]^+$ and $[\text{C}_{14}\text{H}_{28}\text{S}_6\text{OAg}]^+$ and octahedral distorted for $[\text{C}_{12}\text{H}_{24}\text{S}_6\text{Ag}]^+$ as was found in the X-ray experiments. This minor effect on the structures can be expected since the counterions are weakly coordinated [41]. Based on these results, the counterions will be disregarded in the following discussion.

Following the study of the structural properties of the pristine Ag^+ -complexes, the Ag ion was replaced by Cd^{2+} (position 2 of STEP III in Fig. 3) and the self-consistent electronic structure of the three molecules, with all atoms in their initial un-relaxed positions, was calculated. Through structural optimization (position 3), the metal coordination found was

Fig. 3 Computational procedure used to obtain the structures before and after the $^{111}\text{Ag} \rightarrow ^{111}\text{Cd}$ decay using $[\text{C}_{12}\text{H}_{24}\text{S}_6\text{X}]^n$ as an example. Atomic colors conventions: gold S, black C, blue Ag, green Cd. The numbers inside the crown thioethers are the S–Ag and S–Cd distances in Å (also shown in Table 1)

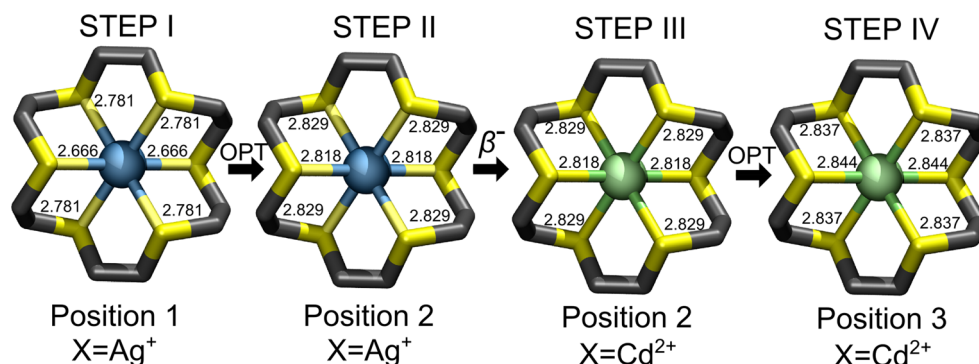


Table 1 Metal coordination bond-lengths (in Å) obtained through X-ray diffraction (position 1, Ref. [22, 27]) and optimized from density functional theory (position 2-Cl, geometry optimization considering the counterions; and position 2, geometry optimization considering the total charge state of molecule). Position 3 corresponds to the structure distorted by the replacement of Ag^+ by Cd^{2+}

		X= Ag^+ Position 1	X= Ag^+ Position 2-Cl ^a	X= Ag^+ Position 2	X= Cd^{2+} Position 3	
[C ₁₂ H ₂₄ S ₆ X]	S1-X	2.6665(12)	2.847	2.818	2.844	
	S2-X	2.6665(12)	2.721	2.818	2.844	
	S3-X	2.7813(10)	2.961	2.829	2.837	
	S4-X	2.7813(10)	2.757	2.828	2.837	
	S5-X	2.7813(10)	2.757	2.828	2.837	
	S6-X	2.7813(10)	2.960	2.829	2.837	
	Cl-X	6.976	6.613	-	-	
	[C ₁₃ H ₂₆ S ₆ OX]	S1-X	3.553(0)	3.933	3.684	2.907
		S2-X	2.644(2)	2.716	2.722	2.890
		S3-X	2.573(2)	2.688	2.666	2.821
S4-X		3.269(0)	3.079	3.279	2.915	
S5-X		2.655(3)	2.749	2.804	2.884	
S6-X		2.551(2)	2.641	2.600	2.812	
Cl-X		5.640	5.284	-	-	
[C ₁₄ H ₂₈ S ₆ OX]	S1-X	2.578(2)	2.664	2.662	2.835	
	S2-X	4.502(2)	4.865	4.626	2.999	
	S3-X	2.597(2)	2.832	2.710	2.820	
	S4-X	2.586(2)	2.607	2.634	2.887	
	S5-X	3.719(2)	3.858	3.985	2.924	
	S6-X	2.598(2)	2.642	2.662	2.840	
	Cl-X	5.046	4.281	-	-	

^a Optimization geometry considering the counterions, represented by Cl

octahedral distorted in all cases. Although the [C₁₃H₂₆S₆OCd]²⁺ and [C₁₄H₂₈S₆OCd]²⁺ initial structures (position 2) are tetrahedral distorted, the S–Cd bond lengths, initially smaller than 3.0 Å, were enlarged, whereas the distances initially larger than 3.0 Å were shortened, which leads to the final optimized octahedral distorted Cd²⁺ coordination. In the case of [C₁₂H₂₄S₆Cd]²⁺, the S–Cd bond lengths remain nearly unaltered after structural optimization, which can be attributed to the small size of the C₁₂H₂₄S₆ ligand, which has lower flexibility to change its coordination sphere.

Table 2 lists the EFG tensors obtained at the Ag sites. Since no Ag isotopes were used as probes in TDPAC experiments [23], these results cannot be compared with experimental data. Nevertheless, they can be used to clarify the differences in the hyperfine properties originated by substitution of the Ag⁺ ion by Cd²⁺. The EFG tensors at Ag sites were derived from two different sets of positions: the experimental coordinates (position 1, see Fig. 3) and at those predicted by DFT (position 2 in Table 1). As can be seen in Table 2, in all cases, the V_{zz} values at the Ag⁺ sites for the experimental positions are approximately only $1 \times 10^{21} \text{ V m}^{-2}$ larger than those obtained for the optimized structures—a small difference. The asymmetry parameter η is more sensitive to fine details of the structure. The EFG tensors at the Cd²⁺ site in the Ag⁺ optimized structure (position 2) and after structure relaxations (position 3) are shown in Table 3. The replacement of Ag⁺ by Cd²⁺ (position

2 in Tables 2, 3) leads to an overall increase in the values (up to $3.0 \times 10^{21} \text{ V m}^{-2}$). Considering that the EFGs at Ag⁺ and Cd²⁺ sites were calculated for the same structures, these changes originate solely from the different electronic structures of Ag and Cd. Interestingly, after structural optimizations (position 3, Table 3), the values at the Cd²⁺ site in [C₁₃H₂₆S₆OCd]²⁺ and [C₁₄H₂₈S₆OCd]²⁺ are reduced by one-half and the η values are enlarged to about 0.5–0.8. On the other hand, in the case of [C₁₂H₂₄S₆Cd]²⁺, V_{zz} and η values remain almost unchanged, which is due to the fact that

Table 2 V_{zz} and asymmetry parameter η at the Ag⁺ sites in [C₁₂H₂₄S₆Ag]⁺, [C₁₃H₂₆S₆OAg]⁺ and [C₁₄H₂₈S₆OAg]⁺ complexes. Electric field gradient (EFG) calculations were performed using the experimental X-ray (position 1 in Fig. 3) and optimized (position 2 in Fig. 3) structures

Complex	X-Ray ^a Position 1		Position 2	
	V_{zz} ^b	η	V_{zz} ^b	η
[C ₁₂ H ₂₄ S ₆ Ag] ⁺	6.5	0.6	5.4	0.1
[C ₁₃ H ₂₆ S ₆ OAg] ⁺	9.1	0.7	8.2	0.4
[C ₁₄ H ₂₈ S ₆ OAg] ⁺	8.7	0.3	7.8	0.2

^a [22, 27]

^b In units of 10^{21} V m^{-2}

Table 3 V_{zz} and asymmetry parameter η at Cd^{2+} sites for $[\text{C}_{12}\text{H}_{24}\text{S}_6\text{Cd}]^{2+}$, $[\text{C}_{13}\text{H}_{26}\text{S}_6\text{OCd}]^{2+}$ and $[\text{C}_{14}\text{H}_{28}\text{S}_6\text{OCd}]^{2+}$ complexes in Ag^+ (position 2) and Cd^{2+} (position 3) optimized structures

Complex	Position 2		Position 3	
	V_{zz}^a	η	V_{zz}^a	η
$[\text{C}_{12}\text{H}_{24}\text{S}_6\text{Cd}]^{2+}$	7.3	0.1	7.0	0.0
$[\text{C}_{13}\text{H}_{26}\text{S}_6\text{OCd}]^{2+}$	10.9	0.3	5.5	0.8
$[\text{C}_{14}\text{H}_{28}\text{S}_6\text{OCd}]^{2+}$	10.8	0.2	5.2	0.5

^a In units of 10^{21} V m^{-2}

the metal coordination sphere did not change upon structural relaxation.

The main experimental EFG results available in the literature were obtained using the TDPAC technique [23, 42] in different temperature and environmental conditions, and are summarized in Table 4. The complex $[\text{C}_{12}\text{H}_{24}\text{S}_6\text{Cd}]^{2+}$ was measured in frozen solution (THF) at different temperatures. Fairly good agreement between theory and experiment, for both relaxed and un-relaxed structures, can be observed by comparing the results shown in Tables 3 and 4. Since the present calculations predicted that Cd^{2+} does not introduce important structural distortions in the molecule when replacing an Ag^+ ion, these agreements reflects the ionic character of the EFG in this case. On the other hand, $[\text{C}_{14}\text{H}_{28}\text{S}_6\text{OCd}]^{2+}$ was measured in a crystalline environment at -261°C and 50°C . In this case, the EFG depends strongly on the structural relaxations induced by the Cd^{2+} ion. Comparing the experimental results and our predictions for the EFG (Table 3), we found excellent agreement when the un-relaxed structure is considered (position 2). $[\text{C}_{13}\text{H}_{26}\text{S}_6\text{OCd}]^{2+}$ was measured in a frozen liquid and in a crystal environment. In the latter case, analogous to the $[\text{C}_{14}\text{H}_{28}\text{S}_6\text{OCd}]^{2+}$ system, excellent agreement between theory and experiments was found when the un-relaxed structure was considered. This intriguing behavior can be traced back to the characteristics of the $^{111}\text{Ag} \rightarrow ^{111}\text{Cd}$ probe. ^{111}Ag decays via a β^- process to the 342 keV excited state of ^{111}Cd (see Fig. 2), which has a half-life of 27 ps and,

after this time, the ^{111}Cd nuclei decays by γ emission. The emission of this first γ -ray populates the intermediate $I = 5/2 + (245 \text{ keV excited state})$ of ^{111}Cd and the emission of the second γ -ray depopulates it. During the lifetime of this intermediate level ($\lambda = 84.5 \text{ ns}$, the time window of the measurement is around four times this value), its nuclear quadrupole moment interacts with the extra-nuclear environment (the electronic charge distribution). This (hyperfine) interaction perturbs the spatial and temporal correlations of the emitted γ -rays [15, 16, 25, 26] and is proportional to the EFG (see Fig. 2). The 27 ps half-life of the 342 keV state of ^{111}Cd is the temporal delay between the transition $^{111}\text{Ag} \rightarrow ^{111}\text{Cd}$ and the opening of the time window of the TDPAC measurement. If the relaxation of the molecular structure is completed before the emission of the first γ -ray (i.e., the rearrangement of the structure around the Cd ion is completed in less than 27 ps) the probes will “observe” a static surrounding the equilibrium configuration of the structures. On the other hand, if the time necessary to complete the structural relaxation around the Cd ion is much larger than the time window of the measurement (84.5 ns), the measured EFG will also be static, and correspond to the un-optimized structure (position 2 in Fig. 3). In an intermediate situation, when the time necessary to complete the structural distortions is of the order of 85 ns or less, the structure around the probes (and, as a consequence, the EFGs) will change during the time window of the measurement. In this case, the TDPAC spectra will reflect the “snapshot” distribution of structures. Based on this discussion and the large EFG distributions observed in the TDPAC spectra (δ in Table 4), we conclude that the observed EFGs correspond to the second and/or third cases, i.e., that the structural relaxations are not completed before the opening of the TDPAC time window. This indicates a lower limit for the relaxation times.

Finally, the case of $[\text{C}_{13}\text{H}_{26}\text{S}_6\text{OCd}]^{2+}$ in a frozen liquid environment (DMSO, see Table 4) shows that the EFG tensor depends on the molecular environment. V_{zz} decreases from $11.32 \times 10^{21} \text{ V m}^{-2}$ (crystalline environment) to $8.25 \times 10^{21} \text{ V m}^{-2}$, a value that is also consistent with the relaxed structure (position 3, Table 3). Since the EFGs decrease when

Table 4 Experimental results obtained from Refs. [23, 42] for the time-differential perturbed γ - γ angular correlations (TDPAC) measurements of the EFG at ($^{111}\text{Ag} \rightarrow ^{111}\text{Cd}$) sites. ω_Q , V_{zz} , and η are defined in the text. Tetrahydrofuran (THF) and dimethylsulfoxide (DMSO) are solvents and, in these cases, the complexes are in frozen solution

Complex	Environment	T (°C)	ω_Q (MRad s^{-1})	V_{zz} (10^{21} V m^{-2})	η	δ (%)
$[\text{C}_{12}\text{H}_{24}\text{S}_6\text{Cd}]^{2+}$	THF	-70	29.0(5)	9.20	0.35(1)	8(1)
	THF	-29	27.7(2)	8.79	0.50(3)	4(2)
$[\text{C}_{13}\text{H}_{26}\text{S}_6\text{OCd}][\text{Tosylat}]$	DMSO	-60	26.0(1)	8.25	0.34(9)	6(6)
	Crystal	-266	36.5(2)	11.58	0.52(1)	9(1)
	Crystal	-60	35.7(2)	11.32	0.53(1)	7.0(6)
	Crystal	22	35.7(2)	11.32	0.54(1)	5.8(4)
$[\text{C}_{14}\text{H}_{28}\text{S}_6\text{OCd}][\text{CF}_3\text{SO}_3]$	Crystal	-261	41 (11)	13.01	0.52(7)	24(7)
	Crystal	50	37.2(7)	11.80	0.75(2)	10 fix

the structural relaxations are computed and also decrease going from the crystal to the frozen solution environment, a possible correlation between these two behaviors can be suggested.

Conclusions

Ab initio CP-PAW calculations in the Kohn-Sham scheme of the DFT were applied to investigate metal coordination of $[C_{12}H_{24}S_6X]^n$, $[C_{13}H_{26}S_6OX]^n$ and $[C_{14}H_{28}S_6OX]^n$ (X: Ag^+ , Cd^{2+}) crown thioethers. The structural and hyperfine results allowed direct comparison with experimental results obtained in X-ray diffraction and TDPAC experiments. We found that our ab initio calculations using isolated Ag^+ complexes as model reproduced experimental S-Ag bond lengths fairly well. Replacement of the Ag^+ ion by Cd^{2+} (the TDPAC probe) produces significant structural distortions in the $[C_{13}H_{26}S_6OX]^n$ and $[C_{14}H_{28}S_6OX]^n$ complexes, whereas the structure of $[C_{12}H_{24}S_6X]^n$ is not affected upon substitution. In addition, the EFG values for the Cd^{2+} complex considering different structural and electronic scenarios were compared to experimental TDPAC results reported in the literature. Remarkably, the results presented here reveal that the structures “observed” by the ($^{111}Ag \rightarrow$) ^{111}Cd probes are the unoptimized ones, i.e., the Cd^{2+} complexes in the Ag^+ coordination sphere. This result was discussed in terms of the characteristics of the probe nucleus and the relaxation times, revealing the combination of theory and experiment to be an important tool with which to study metal complex relaxation.

Acknowledgments This work made use of Laboratório de Computação Científica Avançada Universidade de São Paulo (LCCA-USP) and Centro Nacional de Processamento de Alto Desempenho em São Paulo (CENAPAD/SP) computational facilities and was supported financially by São Paulo Research Foundation (FAPESP), Conselho Nacional de Desenvolvimento Científico e Tecnológico (CNPq), Coordenação de Aperfeiçoamento de Pessoal de Nível Superior (CAPES), and partially supported by Universidad Nacional del Noroeste de Buenos Aires (UNNOBA), Consejo Nacional de Investigaciones Científicas y Técnicas (CONICET) under Grant No. PIP0002 and Universidad Nacional de La Plata, “Instituto Nacional de Electrónica (INEO)” and “Avanços, Benefícios e Riscos da Nanobiotecnologia Aplicada à Saúde (RedeNanobiomed)” networks. F.C.D.A.L. acknowledges the FAPESP support (2012/02326-8). The authors acknowledge Ana Maria da Costa Ferreira, Queite de Paula and Vanessa Roberta Rodrigues Cunha for fruitful discussions. The authors also thank the Cambridge Crystallographic Data Base (CCSD) software for the license of awarded to the Consejo Superior de Investigaciones Científicas (CSIC) of Spain.

Compliance with Ethical Standards The authors declare to comply with the ethical standards of the journal.

Conflict of Interest The authors declare that they have no conflict of interest.

References

- Lindoy LF, Meehan GV, Vasilescu IM et al (2010) Transition and post-transition metal ion chemistry of dibenzo-substituted, mixed-donor macrocycles incorporating five donor atoms. *Coord Chem Rev* 254:1713–1725. doi:10.1016/j.ccr.2009.11.012
- Lee E, Lee SY, Lindoy LF, Lee SS (2013) Metallacycles derived from metal complexes of exo-coordinated macrocyclic ligands. *Coord Chem Rev* 257:3125–3138. doi:10.1016/j.ccr.2013.08.002
- Melchior A, Peralta E, Valiente M et al (2013) Interaction of d(10) metal ions with thioether ligands: a thermodynamic and theoretical study. *Dalton Trans* 42:6074–6082. doi:10.1039/c3dt2332c
- Aragoni MC, Arca M, Bencini A et al (2008) Interaction of mixed-donor macrocycles containing the 1,10-phenanthroline subunit with selected transition and post-transition metal ions: metal ion recognition in competitive liquid-liquid solvent extraction of Cu(II), Zn(II), Pb(II), Cd(II), Ag(I), and. *Inorg Chem* 47:8391–8404. doi:10.1021/ic800548p
- Isaad J, El Achari A (2013) A water soluble fluorescent BODIPY dye with azathia-crown ether functionality for mercury chemosensing in environmental media. *Analyst* 138:3809–3819. doi:10.1039/c3an00252g
- Stephen E, Blake AJ, Carter E et al (2012) Redox non-innocence of thioether crowns: elucidation of the electronic structure of the mononuclear Pd(III) complexes $[Pd([9]aneS3)_2]^{3+}$ and $[Pd([18]aneS6)]^{3+}$. *Inorg Chem* 51:1450–1461. doi:10.1021/ic2017006
- Shaw JL, Wolowska J, Collison D et al (2006) Redox non-innocence of thioether macrocycles: elucidation of the electronic structures of mononuclear complexes of gold(II) and silver(II). *J Am Chem Soc* 128:13827–13839. doi:10.1021/ja0636439
- Bieda R, Kitanovic I, Alborzinia H et al (2011) Antileukemic activity and cellular effects of rhodium(III) crown thiaether complexes. *Biometals* 24:645–661. doi:10.1007/s10534-011-9414-9
- Bieda R, Dobroschke M, Triller A et al (2010) Cell-selective, apoptosis-inducing rhodium(III) crown thiaether complexes. *Chem Med Chem* 5:1123–1133. doi:10.1002/cmdc.201000129
- Bratsos I, Mitri E, Ravalico F et al (2012) New half sandwich Ru(II) coordination compounds for anticancer activity. *Dalton Trans* 41:7358–7371. doi:10.1039/c2dt30654a
- Serli B, Zangrando E, Gianferrara T et al (2005) Is the aromatic fragment of piano-stool ruthenium compounds an essential feature for anticancer activity? The development of new ruii-[9]anes3 analogue. *Eur J Inorg Chem* 2005:3423–3434. doi:10.1002/ejic.200500210
- Madureira J, Santos TM (2013) Solution and solid-state spectroscopic characterization of chloro dimethylsulfoxide polythioether ruthenium(II) complexes, complemented with DFT calculations in the gas phase. *J Coord Chem* 66:881–903. doi:10.1080/00958972.2013.770846
- Feng L, Geisselbrecht Y, Blanck S et al (2011) Structurally sophisticated octahedral metal complexes as highly selective protein kinase inhibitors. *J Am Chem Soc* 133:5976–5986. doi:10.1021/ja1112996
- Jomova K, Valko M (2011) Advances in metal-induced oxidative stress and human disease. *Toxicology* 283:65–87. doi:10.1016/j.tox.2011.03.001
- Schatz G, Weidinger A (1996) Nuclear condensed matter physics: nuclear methods and application. Wiley, New York
- Hemmingsen L, Sas KN, Danielsen E (2004) Biological applications of perturbed angular correlations of gamma-ray spectroscopy. *Chem Rev* 104:4027–4062. doi:10.1021/cr030030v
- Łuczowski M, Zeider BA, Hinz AVH et al (2013) Probing the coordination environment of the human copper chaperone HAH1:

- characterization of Hg(II)-bridged homodimeric species in solution. *Chemistry* 19:9042–9049. doi:10.1002/chem.201204184
18. Iranzo O, Chakraborty S, Hemmingsen L, Pecoraro VL (2011) Controlling and fine tuning the physical properties of two identical metal coordination sites in de novo designed three stranded coiled coil peptides. *J Am Chem Soc* 133:239–251. doi:10.1021/ja104433n
 19. Aghabozorg H, Sohrabi B, Mashkouri S, Aghabozorg HR (2012) Ab initio DFT study of bisphosphonate derivatives as a drug for inhibition of cancer: NMR and NQR parameters. *J Mol Model* 18: 929–936. doi:10.1007/s00894-011-1114-4
 20. Latošnička JN, Seliger J, Zagar V, Burchardt DV (2012) A comparative study of the hydrogen-bonding patterns and prototropism in solid 2-thiocytosine (potential antileukemic agent) and cytosine, as studied by ¹H-¹⁴N NQDR and QTAIM/ DFT. *J Mol Model* 18:11–26. doi:10.1007/s00894-011-1021-8
 21. Petersen PAD, Silva AS, Gonçalves MB et al (2014) Cd hyperfine interactions in DNA bases and DNA of mouse strains infected with *Trypanosoma cruzi* investigated by perturbed angular correlation spectroscopy and ab initio calculations. *Biochemistry* 53:3446–3456. doi:10.1021/bi401680h
 22. Alberto R, Nef W, Smith A et al (1996) Silver(I) complexes of the derivatized crown thioether ligands 3,6,9,12,15,18-hexathianadecanol and 3,6,9,13,16,19-hexathiaicosanol. Determination of stability constants and the crystal structures of [Ag(19-aneS6-OH)][CF3SO3] and [Ag(20-aneS6-OH)][BF4]. *Inorg Chem* 35:3420–3427. doi:10.1021/ic951421y
 23. Heinrich F, Ctordecka B, Tröger W (2005) The electric field gradient of ¹¹¹Ag in macrocyclic crown thioethers. *Hyperfine Interact* 158:79–88. doi:10.1007/s10751-005-9012-8
 24. Lima FCDA, Nascimento RR, Gonçalves MB et al (2010) Electric field gradient and electronic properties of crown thioether compounds. *Hyperfine Interact* 197:23–27. doi:10.1007/s10751-010-0246-8
 25. Lurf A, Butz T (1987) Nuclear quadrupole interactions in compounds studied by time differential perturbed angular correlations/distributions. *Hyperfine Interact* 36:275–370. doi:10.1007/BF02395636
 26. Lurf A, Butz T (1987) Nuclear quadrupole interaction and time-resolved Perturbed- γ -Angular correlation spectroscopy: applications in chemistry, materials science, and biophysical chemistry. *New analytical methods*(31). *Angew Chem Int Ed Engl* 26:110–126. doi:10.1002/anie.198701101
 27. Blake AJ, Gould RO, Holder AJ et al (1989) Silver thioether chemistry: synthesis, X-ray crystal structure and redox properties of [Ag([18]aneS6)]⁺ ([18]aneS6 = 1,4,7,10,13,16-hexathiacyclooctadecane). *Polyhedron* 8:513–518. doi:10.1016/S0277-5387(00)80749-4
 28. Petrilli H, Blöchl P, Blaha P, Schwarz K (1998) Electric-field-gradient calculations using the projector augmented wave method. *Phys Rev B* 57:14690–14697. doi:10.1103/PhysRevB.57.14690
 29. Herzog P, Freitag K, Reuschenbach M, Walitzki H (1980) Nuclear orientation of ^{111m}Cd in Zn and Be and the quadrupole moment of the 245keV state. *Z Phys A Atoms Nucl* 294:13–15. doi:10.1007/BF01473117
 30. Pyykko P (2001) Spectroscopic nuclear quadrupole moments. *Mol Phys* 99:1617–1629. doi:10.1080/00268970110069010
 31. Hohenberg P, Kohn W (1964) Inhomogeneous electron gas. *Phys Rev* 136:864–871. doi:10.1103/PhysRev.136.B864
 32. Kohn W, Sham LJ (1965) Self-consistent equations including exchange and correlation effects. *Phys Rev* 140:A1133–A1138. doi:10.1103/PhysRev.140.A1133
 33. Blöchl PE, Först CJ, Schimpl J (2003) Projector augmented wave method: ab initio molecular dynamics with full wave functions. *Bull Mater Sci* 26:33–41. doi:10.1007/BF02712785
 34. Blöchl PE (1994) Projector augmented-wave method. *Phys Rev B* 50:17953–17979. doi:10.1103/PhysRevB.50.17953
 35. Alves-Santos M, Dávila LYA, Petrilli HM et al (2006) Application of standard DFT theory for nonbonded interactions in soft matter: prototype study of poly-para-phenylene. *J Comput Chem* 27:217–227. doi:10.1002/jcc.20326
 36. Haas H, Petrilli H (2000) Quadrupole moments of the halogen nuclei. *Phys Rev B* 61:13588–13592. doi:10.1103/PhysRevB.61.13588
 37. Car R, Parrinello M (1985) Unified approach for molecular dynamics and density-functional theory. *Phys Rev Lett* 55:2471–2474. doi:10.1103/PhysRevLett.55.2471
 38. Perdew JPI, Burke K, Ernzerhof M (1996) Generalized gradient approximation made simple. *Phys Rev Lett* 77:3865–3868. doi:10.1103/PhysRevLett.77.3865
 39. Errico LA, Rentería M, Petrilli HM (2007) Augmented wave ab initio EFG calculations: some methodological warnings. *Phys B Condens Matter* 389:37–44. doi:10.1016/j.physb.2006.07.013
 40. Gonçalves MB, Di Felice R, Poleshchuk OK, Petrilli HM (2008) Ab initio study of the EFG at the N sites in imidazole. *Hyperfine Interact* 181:53–58. doi:10.1007/s10751-008-9700-2
 41. Krossing I, Raabe I (2004) Noncoordinating anions—fact or fiction? A survey of likely candidates. *Angew Chem Int Ed Engl* 43: 2066–2090. doi:10.1002/anie.200300620
 42. Ctordecka B (1999) Rigidity and adaptivity of metal sites in macromolecules. Universität Leipzig, Leipzig